Article

Study on Performance of Locomotive Diesel Engine Fueled with Biodiesel Using Two Miller Cycle Technologies

Feng Jiang [1,2]**, Junming Zhou** [1]**, Jie Hu** [1,2,*]**, Xueyou Tan** [1]**, Wentong Cao** [1] **and Zedan Tan** [1]

[1] School of Mechanical and Automotive, Guangxi University of Science and Technology, Liuzhou 545006, China; 100001086@gxust.edu.cn (F.J.); a13078027926@163.com (J.Z.); tanxueyou123@163.com (X.T.); cao12580159@163.com (W.C.); 17754551926@163.com (Z.T.)
[2] Guangxi Key Laboratory of Automobile Components and Vehicle Technology, Guangxi University of Science and Technology, Liuzhou 545006, China
[*] Correspondence: 100001078@gxust.edu.cn

Abstract: In this paper, the simulation model was established based on GT-Power software, and a scheme using the Miller cycle based on biodiesel was proposed. Taking diesel engine 16V265H as the research object, the accuracy of the simulation model was verified by experiments. Combined with the comparison of physical and chemical characteristics of biodiesel and the experimental analysis of biodiesel under three different combinations, it was concluded that low ratio biodiesel was the best choice to meet the power, economy, and emission performance of diesel. Through the simulation scheme of the two Miller cycles for pure diesel (B0) and biodiesel (B10) under different load conditions at 1000 rpm, the NO_x emission performance of pure diesel in a Miller cycle was significantly improved. On this basis, the comprehensive performance of the two Miller cycles was compared with biodiesel. The results showed that both the Miller cycles could reduce NO_x emission. Combined with other key performances of a diesel engine, the best scheme to improve the performance of the diesel engine was to burn B10 biodiesel and overlap angle the Miller cycle of the variable valve at 30 °CA. The scheme has guiding significance for the application of the 16V265H diesel engine.

Keywords: NO_X; dynamic performance; locomotive diesel engine; Miller cycle

1. Introduction

Since the beginning of the 21st century, the global transportation industry has developed rapidly, especially rail transportation. Rail transportation is the core link in the current market demand [1]. While pursuing economy and power, environmental protection performance is also very important [2]. In this paper, the 16V265H diesel engine will be taken as the research object [3,4], and the research will be carried out from three aspects of diesel power, economy, and emission performance, especially the optimization of soot and nitrogen oxide (NO_x) emissions [5].

In recent years, many researchers have done a lot of research on the application and development of locomotive diesel engine technology as an alternative fuel to pure diesel [6,7]. As renewable energy [8], biodiesel is significantly better than pure diesel in reducing carbon monoxide (CO), hydrocarbon (HC), and particulate matter (PM) [9,10]. However, at present, there is no research on the use of biodiesel for large diesel locomotives of 16V265H [11]. This paper takes this opportunity to reduce fossil energy consumption by burning biodiesel [12], to achieve the effect of environmental protection and energy-saving [13]. However, when pure biodiesel is added to an ordinary diesel engine without any process optimization, it will have a certain negative impact on engine performance and NO_x emission [14], which is about 13% higher than that of pure diesel [15]. The ultimate purpose of the Miller cycle in this study is to reduce NO_x emission of diesel engines [16].

At present, the most effective method to reduce NO_x emission in this direction is the Miller cycle [17]. The Miller cycle is to close the intake valve at a certain angle before the bottom dead center, and the gas entering the cylinder during the intake stroke will obtain an additional expansion during the downward movement of the piston. In this process, the additional expanded gas will reduce the temperature in the cylinder, reduce the average temperature in the cylinder before combustion, and effectively reduce NO_x emission. As the temperature decreases in the combustion process, the working process of the diesel engine also becomes smooth, which effectively reduces the working noise of the diesel engine. Increasing the geometric compression ratio while reducing the effective compression ratio can improve the combustion efficiency, to increase the output power and torque. The NO_x emission will not increase sharply, and the engine components do not have to bear the excessive load, which effectively prolongs the service life of engine components. Compared with conventional diesel engines, the intake pressure of the Miller cycle is higher [18], but the maximum pressure in the cylinder remains unchanged [19]. During the intake stroke, an additional expansion period [20] will be obtained. However, most of the research in this direction is based on the impact of one Miller cycle [21] on engine performance [22]. Wang et al. [23] researched the Miller cycle of marine diesel engine and realized the experimental research on the influence of the Miller cycle combined with EGR on the performance, energy, and exergy of four-stroke marine regulated two-stage turbocharged diesel engine by redesigning camshaft and EGR system. The research shows that under 75% load, the combination of medium Miller timing and medium EGR rate can not only meet the three-level NO_x emission requirements, but also far better than only high EGR rate in fuel economy, opacity, and COVIMEP. Guan et al. [24] conducted a study on Miller cycle operation by delayed inlet valve closing (LIVC) with and without EGR in a single-cylinder heavy-duty diesel engine equipped with a variable valve drive (VVA) system. The research shows that due to the relatively low engine output nitric oxide (NO) emission, the introduction of EGR allows the engine to operate with higher corrected net indicated efficiency (NIE) or lower specific total fluid consumption than the benchmark without EGR. Wei et al. [25] analyzed the influence of early inlet valve closing (EIVC) Miller cycle on low and medium load combustion and emission of marine diesel engines. The research showed that appropriate EIVC would reduce the pressure, temperature, and NO emission in the cylinder. When the load was 50%, the nitric oxide emission was reduced by 17.8%, and when the load was 25%, the NO emission was reduced by 14.9%. Li et al. [26] verified the diesel engine method of using the Miller cycle, turbocharger, and ethanol to reduce NO_x and particulate emissions based on a numerical method and model. The results showed that the Miller cycle did reduce NO_x emission to a certain extent. Compared with the traditional diesel cycle, the NO_x emission value of the Miller cycle was reduced by 8.5–12.9%. The Miller cycle, as an effective means to reduce NO_x emission of diesel engine, is gradually being widely used. At present, the main research work at home and abroad focuses on some large natural gas engines and heavy diesel engines for power generation. After consulting relevant literature, researchers at home and abroad mainly focus on the impact of using one Miller cycle mode on engine performance, while there is less research on the impact of multiple the Miller cycle modes on engine performance. This paper studies the influence of biodiesel on the performance of locomotive diesel engines through two different Miller cycle modes of variable cam profile and variable valve overlap angle, compares the effects of the two Miller cycle modes and selects the better Miller cycle implementation mode. Its research results will fill the gap in the use of biodiesel for large diesel locomotives [27], effectively reduce the use of petrochemical energy [28] and improve the ecological environment [29].

In conclusion, the numerical simulation analysis of diesel engines has outstanding economic advantages through an accurate mathematical model framework [30], which can make a great contribution to the cost-saving of the experimental team. In this paper, the power, economy, and emission performance of the simulated diesel engine are optimized by burning biodiesel under the conditions of the two Miller cycles [31].

This paper mainly studies the biodiesel combustion of the 16V265H diesel engine based on two different Miller cycle B10 concentrations at 1000 rpm and 100% load. The parameters of diesel engine power, torque, fuel consumption, and NO_x emission are taken as the result variables of the model. The Miller degree of diesel engine (including the advanced closing angle of inlet valve in the variable cam profile Miller cycle scheme, the overlap angle of the variable valve, and the translation angle of inlet valve lift curve in the Miller cycle scheme) is taken as the independent variable of the optimization model to determine the optimal Miller degree (°CA) of the 16V265H diesel engine under 1000 rpm and 100% load conditions. This study will provide a method reference for the follow-up research work of the Miller cycle, and its research results have certain engineering application value.

2. Numerical Approaches

The working process in the cylinder of a large railway locomotive diesel engine is very complex, which is generally divided into heat transfer, flow, physical and chemical processes. Its basic differential equation is one of the basic equations that must be followed in simulation calculation. At the same time, the establishment of a biodiesel fuel depot is also very important. The key is to improve its fuel depot according to the thermodynamic parameters and attributes of biodiesel with different ratios. The fuel depot is built mainly by improving the "FluidLiqIncompress" module through GT suite software. It mainly involves the relationship between the physical and chemical parameters of biodiesel fuel and its constant pressure-specific heat and heat transfer coefficient temperature obtained through semi-empirical formula [32].

2.1. Theory of Diesel Engine Working Process

The diesel engine simulation software in this paper is based on the GT-Power module. The core equation in the simulation process is the basic differential equation of the diesel engine in the cylinder. This equation can be extended to other models such as combustion and exhaust. The working medium state in the cylinder of the diesel engine is described by cylinder pressure: P, temperature: T, and mass: M. To correlate the cylinder working process into one, it is necessary to meet the energy conservation equation, mass conservation equation, and ideal gas state formula [33].

(1) Energy conservation equation:

The following equation can be obtained from the first law of thermodynamics [33]:

$$\frac{dU}{d\varphi} = \frac{dQ_B}{d\varphi} + \frac{dm_s}{d\varphi}h_s - \frac{dm_e}{d\varphi}h_e - \frac{dQ_w}{d\varphi} - p\frac{dV}{d\varphi} \tag{1}$$

where U is the internal energy of the overall system, kJ; Q_B is the heat energy released by the combustion of fuel in the cylinder, kJ; Q_W is the heat energy exchanged through each interface of the cylinder system, kJ; H_s and H_e are the specific enthalpies of working medium at inlet valve and outlet valve, respectively.

(2) Mass conservation equation:

According to the mass conservation theorem [34], the mass change of working medium in the thermodynamic system is equivalent to the total mass exchanged at the model boundary of the thermodynamic system $\sum_j dm_j$, that is:

$$dm = \sum_j dm_j \tag{2}$$

Considering that the working medium does not have leakage and other factors, and the working medium mass exchanged through the simulation boundary of the thermodynamic system is: the mass of the working medium entering the cylinder in m_S, the mass of the

exhaust gas flowing out of the cylinder in me, and the mass of the burned fuel in the cylinder in m_B, the mass conservation equation is determined through the above:

$$\frac{dm}{d\varphi} = \frac{dm_s}{d\varphi} + \frac{dm_e}{d\varphi} + \frac{dm_B}{d\varphi} \tag{3}$$

(3) Equation of state of an ideal gas:

$$pV = mRT \tag{4}$$

where m is the mass of working medium in the cylinder, kg; V is the working volume of the cylinder, m^3; p is the working medium pressure in the cylinder, Pa; T is the temperature of working medium in the cylinder, K; and R is the gas constant.

2.2. Establishment of Biodiesel Fuel Bank

2.2.1. Biodiesel Density Coefficient

The shape or spatial location of matter will not change due to the change of density, and the factor of density change is the state of different temperatures and pressure. The GTI computational model was chosen for the biodiesel fuel pool in the GT-Suite modeling process based on the characteristics of this diesel engine, and the corresponding density of states equation was:

$$\rho(P, T) = a_0 + \frac{[P + a_1 \cdot T + a_2]^{(a_3 + 1)}}{a_3 + 1} + P[a_4 \cdot T^{a_5} + a_6] + a_7\sqrt{T} \tag{5}$$

The coefficient values a_1, a_2, a_3, a_4, a_5, a_6, and a_7 are set in the software as constant pressure-specific heat values.

2.2.2. Fitting Coefficient of Steam Enthalpy of Biodiesel

An important state parameter characterizing the energy of the material system in thermodynamics is enthalpy. Fuel enthalpy includes specific enthalpy, apparent enthalpy, and formation enthalpy. The specific enthalpy at a specific temperature is equal to the formation enthalpy plus enthalpy change at the reference temperature (298 K).

According to the calculation formula of enthalpy and the calculation formula of specific constant pressure heat capacity $c_{p_0} = \frac{dh}{dT}$ [35], the approximate value of the enthalpy fitting coefficient of biodiesel can be deduced.

$$\Delta h = h_2 - h_1 = c_{p0}(T_2 - T_1) \tag{6}$$

The enthalpy of fuel at standard atmospheric pressure and different temperatures is calculated by the following equation:

$$h = h_{ref.lip} + a_1(T - T_{ref}) + a_2(T - T_{ref})^2 + a_3(T - T_{ref})^3 \tag{7}$$

T_{ref} = 298 K. For biodiesel, the liquid reference enthalpy values are:

$$h_{ref.lip} = h_{ref.vap} - \Delta h_{vaporization} \tag{8}$$

$h_{ref,vap}$ shows the reference enthalpy of biodiesel, and $\Delta h_{vaportzation}$ shows the evaporation heat of biodiesel at standard atmospheric pressure and 298 K temperature. If the reference enthalpy of biodiesel liquid is known, the gas reference enthalpy can be calculated [36].

The constant pressure-specific heat values a_1, a_2 and a_3 can be set in the software. Only the first-order coefficient value needs to be set to establish the fuel depot, so $a_2 = a_3 = 0$. The a_1 values of biodiesel with different proportioning concentrations are shown in Table 1.

Table 1. Coefficient (a_1) of different ratios biodiesel.

Biodiesel Ratio	The First-Order Fuel Coefficient a_1 (kJ/((k·kg))
B100	2762
B50	2406
B20	2193
B10	2121
B0	2020

As the fuel enters the cylinder under high-pressure injection and gradually atomizes from aerosol to droplet state. The evaporation of droplet fuel in the cylinder leads to the evaporation of fuel into the gaseous state. The change of fuel properties leads to the change of enthalpy value. The literature showed that the latent heat of vaporization of biodiesel at 298 K is 420 kJ/kg. Due to the exothermic process during the formation of gasification, the enthalpy of liquid and gaseous fuel is closely related [37]. Table 1 shows the a_1 coefficient values of different biodiesel ratios. According to the above formula, the a_1 coefficient values of biodiesel steam can be obtained, as shown in Table 2.

Table 2. Evaporation coefficient (a_1) of different ratios biodiesel.

Biodiesel Ratio	The First-Order Coefficient Value of Steam a_1 (kJ/((k·kg))
B100	2342
B50	2034
B20	1909
B10	1855
B0	1770

2.2.3. Thermal Conductivity of Biodiesel

At present, the components of biodiesel on the market are different, and there are some differences, but the main components are saturated or unsaturated fatty acid methyl esters, including methyl stearate, methyl linoleate, methyl linolenate, methyl palmitate, etc. In this paper, biodiesel is made of soybean oil, and its sufficiency and properties are shown in the Table 3. The thermal conductivity of the pure material liquid is constant at a certain temperature, so the thermal conductivity of biodiesel liquid is estimated by the power-law method [38], and the relationship is as follows:

$$\lambda = \left(\sum_i w_i \lambda_i^{-2}\right)^{-1/2} \tag{9}$$

where λ_i is the thermal conductivity of the pure substance, and w_i is the mass fraction of the pure substance in biodiesel [39].

Table 3. The main composition and the properties of biodiesel.

Project	Methyl Stearate	Methyl Linoleate	Methyl Linolenate	Methyl Palmitate	Methyl Oleate
Chemical formula	$C_{19}H_{38}O_2$	$C_{19}H_{34}O_2$	$C_{19}H_{32}O_2$	$C_{17}H_{34}O_2$	$C_{19}H_{36}O_2$
Molecular weight (g/mol)	298	294	292	270	296
Double bond number	0	2	3	0	1
Content (%)	4.9	54.4	6.9	10.6	24.8

According to the relevant knowledge of thermodynamics, the thermal conductivity of biodiesel vapor is approximately linear with the temperature when the temperature changes little [40,41], so the thermal conductivity of biodiesel vapor can be expressed as:

$$k_1 = k_0[1 + \beta(T - 273)] \tag{10}$$

where k_0 is the thermal conductivity at (273 K), W·m^{-1}·K^{-1}; β is the intercept of linear equation, λ is the thermal conductivity of the material at temperature T (K); and T is the in-cylinder temperature, K.

From the above formula, if you want to find β, as long as the thermal conductivity of the substance at two different temperatures is known, the thermal conductivity of biodiesel at standard temperature (273 K) is 0.0101 W·m^{-1}·K^{-1} and that at 373 K is 0.0162 W·m^{-1}·K^{-1}. Furthermore, according to the semi-empirical formula of temperature and thermal conductivity, the thermal conductivity of biodiesel at 298 K–486 K can be calculated. As shown in Table 4, the thermal conductivity of biodiesel increases with the increase of temperature [42].

Table 4. The relationship between temperature and thermal conductivity of biodiesel.

Temperature (K)	Thermal Conductivity (W/(m·K))
298	0.0116
329	0.0135
397	0.0177
416	0.0188
486	0.0237

2.2.4. Viscosity of Biodiesel

The viscosity of biodiesel changes with the change of its physical state. Under low pressure, the viscosity of aerosol biodiesel can be calculated according to the following formula [43]:

$$\mu_0 = \frac{5\sqrt{\pi MRT}}{16\pi\sigma^2\Omega_v} \tag{11}$$

where M is the molecular weight of biodiesel vapor; R is the gas constant; T is the temperature of aerosol biodiesel; σ^2 is the collision diameter of biodiesel vapor molecules; Ω_V is the collision integral of biodiesel vapor molecules [44].

Where Ω_V can be calculated by the following formula:

$$\Omega_v = \frac{A}{(T^*)^B} + \frac{C}{\exp(DT^*)} + \frac{E}{\exp(FT^*)} + \frac{\mu_p^4}{20\kappa^2\sigma^6 T^*} \tag{12}$$

$$\sigma^{1/3} = 2.36545 - 0.08778w \tag{13}$$

$$T^* = \frac{k_B T}{\kappa} \tag{14}$$

In the formula, the values of A, B, C, D, E, and F are 1.16145, 0.14874, 0.52487, 0.77320, 2.16178, and 2.43787, respectively, μ_P is the dipole moment of biodiesel vapor molecules [45,46], D. According to the data [47], it can be obtained: 1.85. σ is determined by the eccentricity factor and critical parameters. P_C is the critical pressure, bar; its value is 11.5 bar. T_C is the critical temperature, K; its value is 792.8 K, and w = 0.7; T^* is dimensionless temperature, K; k_B is the Boltzmann constant. κ is the characteristic energy of biodiesel vapor (the value is equal to the critical temperature), and the data are obtained: Boltzmann constant and κ 1.2593 and 792.8, respectively [48].

2.3. Engine Specifications

According to the emission and power requirements, the 16V265H diesel engine is tested at the speed of 8 handle positions. Each handle position has the corresponding speed and power value. The determined power is fed back to the diesel electro-mechanical injection system to provide the response and realize a circulating fuel supply. At the same time, the diesel engine drives the motor to rotate and the motor generates corresponding power. When the diesel engine speed reaches 1000 rpm, if the diesel engine power cannot

meet the motor power at this time, the motor will reverse inhibit the increase of diesel engine speed and maintain the speed of 1000 rpm. Therefore, the motor is divided into different power gears, which can ensure that the diesel engine has an accurate circulating oil supply at different handle positions (handle positions 5~8) at 1000 rpm. At the same time, this paper uses the engine simulation software GT-Power to simulate the 16V265H diesel engine. The modeling is shown in Figure 1, and the main performance parameters of the diesel engine are shown in Table 5.
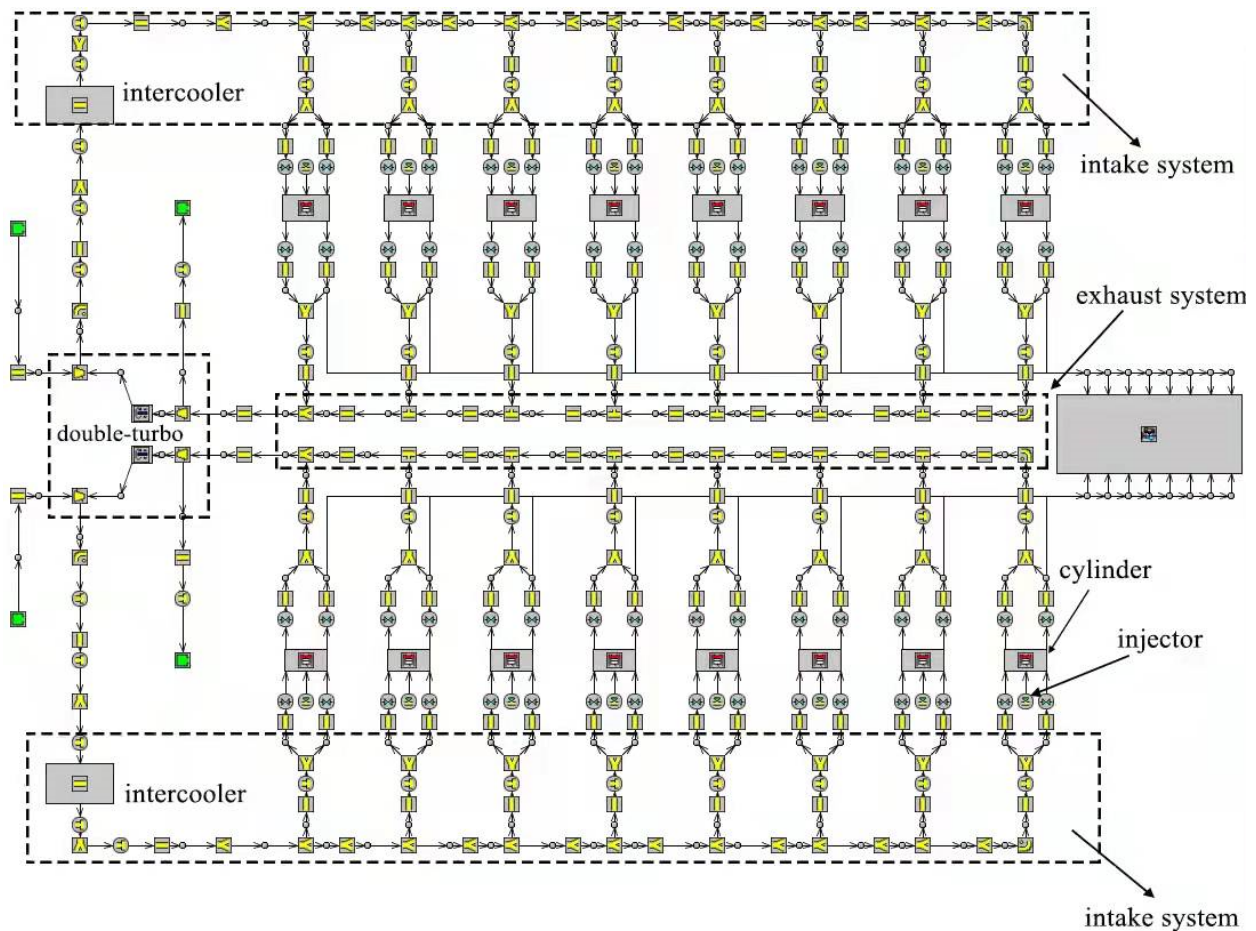
Figure 1. Simulation model of the entire diesel engine.

**Table 5.** The main technical parameters of diesel engine.

| Model	16V265H
Type	4-stroke, 16-cylinder, V-shape, 45°
Cylinder bore × trip	265 × 300 mm
Total displacement	264.74 L
Compression ratio	15.4
Calibration power	4660 kW
Calibration speed	1000 rpm

3. Results and Discussion

3.1. Model Reliability Analysis

To further verify the accuracy of the established simulation model, the simulation calculation of the 16V265H diesel engine burning pure diesel under the working condition of corresponding speed at each handle position is carried out, the variation curve of power

and maximum burst pressure in the cylinder with speed is obtained, and the simulation values are compared with the test values, as shown in Figures 2 and 3.
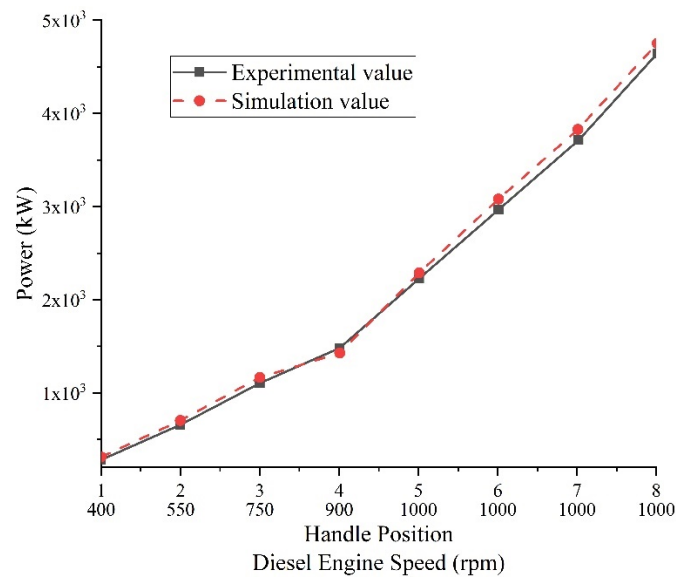
Figure 2. Comparison of power values.
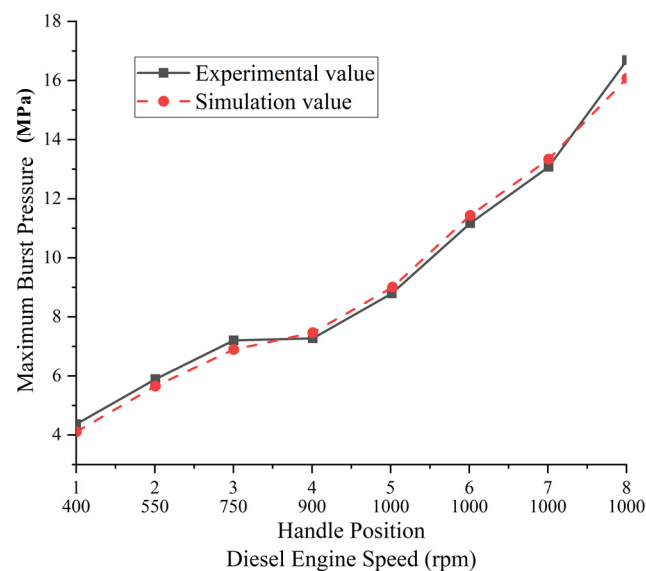
Figure 3. Comparison of maximum burst pressure.

It can be seen from Figures 2 and 3 that the power simulation value reaches the maximum at the handle position of 8 and 1000 rpm, and the maximum burst pressure simulation value in the cylinder reaches the maximum at the handle position of 8 and 1000 rpm. According to the simulation principle, the corresponding one-dimensional simplified treatment is carried out for the diesel engine in the calculation process, and the inlet and exhaust pipe length of the diesel engine is empirically discretized based on the empirical value. At the same time, the relevant models used in the simulation calculation, such as spray model and combustion model, are all empirical models. There is a certain error in the working process of the actual diesel engine. Due to the superposition of the errors, there is a certain error between the power value and the maximum explosion pressure value, and the error is within 6%. Therefore, the model has certain accuracy and can be used to simulate and analyze the performance of 16V265H diesel engines, and the

simulation software has many application examples in engine performance simulation, which is feasible [49].

3.2. Selection of Biodiesel Concentration

3.2.1. Comparison of Physicochemical Properties of Biodiesel with Different Ratios

Biodiesel is a kind of green and renewable energy, which can be used for the internal combustion engine [50–52]. Compared with ordinary diesel, biodiesel has obvious advantages. At home and abroad, biodiesel is very optimistic about the application and development of diesel technology as an alternative fuel to diesel, and a lot of research has been done. To compare the improvement of the diesel engine performance by biodiesel and pure diesel with a different ratio, first analyze its physical and chemical characteristic values, including density, cetane number, and kinematic viscosity, which will affect its diesel power, economy, and emission performance. The experiment shows the optimal ratio concentration of biodiesel with a different ratio in a 16V265H diesel engine.

(1) Density

Density is the quality of substance contained in unit volume. Density is one of the most important indexes in the physical and chemical characteristics of fuel. According to the national standard, if the density of vehicle diesel is in the range of 820~860 kg/m^3, it is regarded as a qualified product. It can be seen from Table 6 that the density of petrochemical diesel is less than that of biodiesel. The density of biodiesel with different ratios formed by mixing the two fuels increases with the increase of ratio. When the ratio of biodiesel exceeds 80%, it exceeds the relevant national standards for the use of vehicle diesel. Therefore, the current market uses low ratio biodiesel.

Table 6. Comparison of physical and chemical characteristics of diesel and biodiesel.

Project	Quality Index				
	B0	B10	B20	B50	B100
Density (20 °C)/(kg/m^3)	821.8	827.4	832.7	849.6	946.6
Sulfur content (mass fraction)/%	0.0234	0.0187	0.0143	0.0105	0.0013
Kinematic viscosity (40 °C)/(mm^2/s)	3.67	4.51	4.71	5.31	6.01
Cetane number	53.6	54.2	55.3	57.6	60.4

(2) Cetane number

Cetane number is an important index of ignition performance of the fuel in a compression ignition engine. A too high cetane number will lead to insufficient fuel combustion, resulting in black smoke and reduced fuel economy. If the cetane number is too low, it will make it difficult to start the engine and reduce the power. It can be seen from Table 6 that the cetane number of pure diesel is the lowest. With the increase of biodiesel concentration ratio, the cetane number also increases, and the larger the concentration ratio is, the greater the increase range is. Therefore, low ratio biodiesel is the best.

(3) Kinematic viscosity

Another important parameter for evaluating combustion is kinematic viscosity, which is mainly reflected in the ability of fluid to resist shear. Viscosity has an important influence on fuel injection quantity, atomization quality, penetration distance, and lubrication of precision coupling. The larger the viscosity, the easier it is to atomize the fuel into the cylinder, resulting in engine wear and spray particle size. If the viscosity is too small, the wear of related components such as fuel injection nozzle and oil pump will be intensified, affecting the service life of parts. It can be seen from Table 6 that with the increase of biodiesel volume ratio, the kinematic viscosity of mixed fuel gradually increases. Therefore, the low ratio biodiesel is the best [53].

3.2.2. Analysis of Biodiesel with Different Proportioning Concentrations

According to the test of the 16V265H diesel engine burning pure diesel, the test is carried out by burning B10, B20, and B50 biodiesel under eight different handle positions without changing any structural parameters and in the best fuel consumption mode, and the data of fuel consumption, torque, NOx and smoke emission under three ratios of biodiesel was obtained. Considering the physical and chemical characteristics of B100 pure biodiesel, complex maintenance problems such as shutdown maintenance of the 16V265H diesel engine due to nozzle blockage can easily occur, as well as practical problems such as difficult cleaning of the fuel passage. Therefore, the highest proportion of biodiesel with different proportions is limited to B50.

(1) Fuel consumption

As shown in Figure 4, the fuel consumption curve of biodiesel with various ratios under different rotating speeds is shown. It can be seen from the figure that the fuel consumption of pure diesel and biodiesel with various ratios has an obvious downward trend when the rotating speed increases. The fuel consumption rate under different rotating speeds is B50 > B20 > B10 > pure diesel (B0). It is intuitively felt that the difference between B50 fuel consumption and B0 fuel consumption reaches the peak at 400 rpm. The fuel consumption of B50 is about 13% higher than that of B20, and that of B20 is about 1.8% higher than that of B10 under the condition of 1000 rpm. The reason for the fuel consumption trend is that when the diesel engine works at low speed, the optimum temperature in the cylinder has not been reached, and combined with the physical and chemical characteristics of biodiesel, the low calorific value is lower than that of pure diesel. It will further produce an endothermic phenomenon, reduce the temperature in the cylinder again, resulting in insufficient combustion and increased fuel consumption. This is roughly the same as the experimental results of Geng et al. [54].
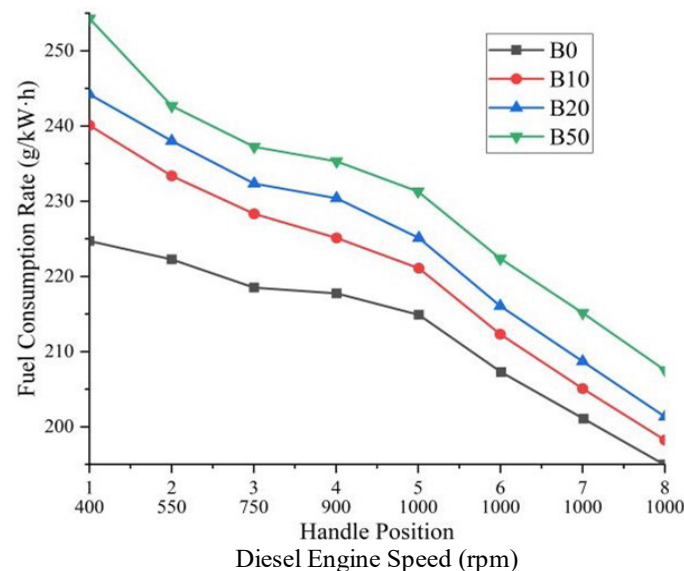

Figure 4. The fuel consumption curve of biodiesel with various ratios at different speeds.

(2) Torque

As shown in Figure 5, the torque curve of biodiesel with various ratios under different speed conditions is shown. It can be seen from the figure that the torque values of pure diesel and biodiesel with various ratios are roughly the same at each speed. The torque values of pure diesel (B0) > B10 > B20 > B50 at different speeds are about 1.6%, 3.2% and 8.0%, respectively. The main reason for the decline in the physical and chemical characteristics of biodiesel with high density and low calorific value. When the fuel injection quantity remains unchanged, the torque of biodiesel with a high ratio such as B50

will be reduced by about 8%, which has a great impact on the power performance of diesel engines. To ensure the power of diesel, it is best to use low ratio biodiesel.
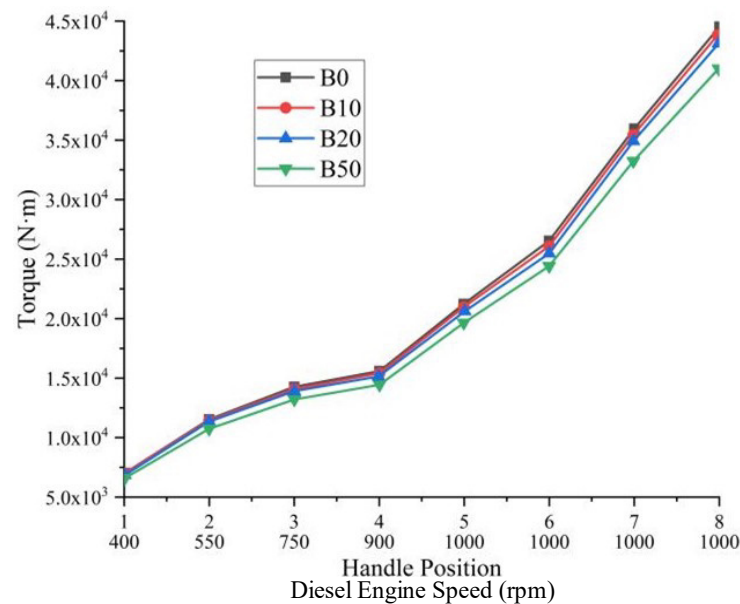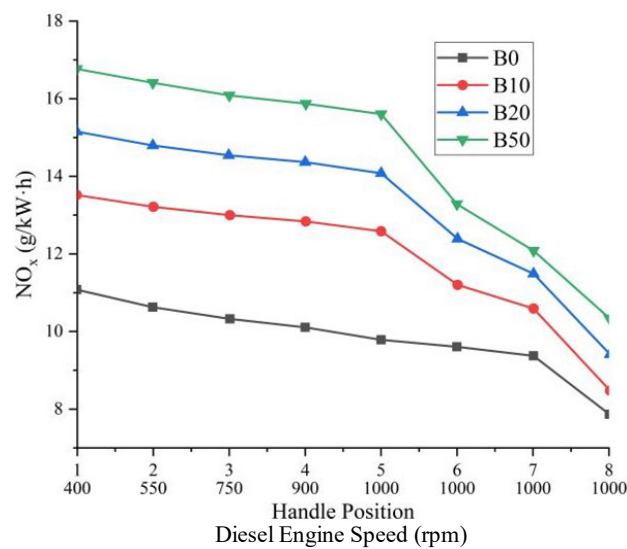

Figure 5. The torque curve of biodiesel with different ratios under various working conditions.

(3) NO_x and soot emissions

As shown in Figures 6 and 7, the NO_x and soot emissions trends of biodiesel fueled with different ratios under different speed conditions are shown. It can be seen from the figure that the NO_x emission of pure diesel decreases gradually at handle positions 1–7, and there is an obvious decline period at handle positions 7–8, while the NO_x emission of biodiesel with different ratios decreases gradually at less than 1000 rpm (handle positions 1–5), and there is also an obvious decline period at 1000 rpm (handle positions 5–8), with a large decline range. The reason is that with the increase of rotating speed, biodiesel is fully mixed, diesel engine emits large power, and NO_x has an obvious downward trend. The trend of soot emission of pure diesel B0 and biodiesel at different speeds is the same, both of which decrease slowly when the speed is less than 1000 rpm, and the decrease range is obvious when the handle is at 5–7. According to the comparison, the average NO_x emission of biodiesel B10 < B20 < B50 is increased by 13.5% compared with B10, B50 is increased by 7% compared with B20, especially at 1000 rpm (handle position 5), B50 is increased by 58.6% compared with pure diesel B0. The average soot emission of biodiesel B10 > B20 > B50 decreased by 12.9% compared with B10 and 8.9% compared with B20. Especially at 1000 rpm (handle position 5), biodiesel B50 decreased by 35.1% compared with pure diesel B0. Since the key of this paper is to reduce NO_x emission, it is best to use low ratio biodiesel. This is consistent with the experiment results of Fan et al. [55].

To sum up, combined with the comparison of physical and chemical characteristics of biodiesel and the test analysis of biodiesel with three different combinations, B10 biodiesel can achieve the best effect in terms of diesel power, economy, and emission performance, followed by B20 biodiesel. In the following, B10 biodiesel will be selected as the basis to analyze the power, economy, and emission performance of diesel engines using two Miller cycles.

Figure 6. The NOx curves of biodiesel with different ratios under various working conditions.
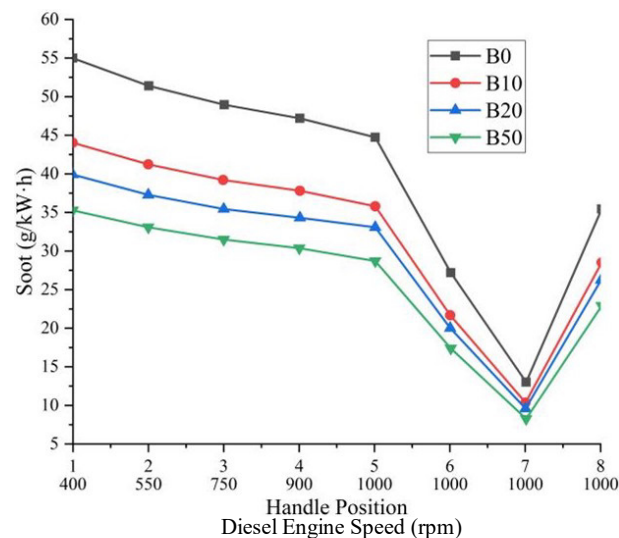
Figure 7. The soot curve of biodiesel with different ratios under various working conditions.

3.3. Application of Two Miller Cycle Analysis

This paper will study two Miller cycles: variable cam profile Miller cycle and variable valve overlap angle Miller cycle.

Using the above simulation model, it will be calculated that under 1000 rpm and 25%, 50%, 75%, and 100% load conditions, the two Miller cycles are applied to pure diesel to compare and analyze the NO_x emission reduction performance. On this basis, B10 biodiesel is used to simulate and analyze the economic, power, and emission performance of diesel engines, and then the optimal Miller cycle scheme is obtained. Of course, when seeking to increase the intake valve advance angle, it is also necessary to appropriately increase the boost pressure. This approach is to prevent the insufficient combustion of biodiesel caused by the lack of intake air in the cylinder, which will worsen the combustion, reduce the power and increase the soot emission.

The two Miller cycles are shown in Tables 7 and 8 below. The Miller degree is 0 °CA, and the crankshaft angle is the initial valve distribution phase, that is, the inlet valve early closing angle, and the fuel injection quantity without the Miller cycle and the Miller cycle shall be the same.

Table 7. Miller cycle scheme of the variable cam line.

Miller Degree (°CA)	Advanced Closing Angle of the Intake Valve (°CA)	Intake Valve Closing Angle (°CA)
0	0	540
10	10	530
20	20	520
30	30	510
40	40	500
50	50	490
60	60	480
70	70	470

Table 8. Overlapping angle Miller cycle scheme of the variable gas valve.

Miller Degree (°CA)	Translation Angle of Intake Valve Lift Curve (°CA)	Intake Valve Closing Angle (°CA)
0	0	540
10	10	530
20	20	520
30	30	510
40	40	500
50	50	490
60	60	480
70	70	470

3.4. Performance Comparison of Two Miller Cycle Modes for Pure Diesel

Firstly, the simulation model is used to calculate the impact of the two Miller cycles on the NO_x emission performance of the 16V265H diesel engines under different working conditions. In the overview, it is mentioned that the Miller cycle is one of the main ways to reduce NOx emission on the market. Therefore, this section only studies the NO_x emission performance, to lay a foundation for the application of the biodiesel Miller cycle in the next section.

(1) Emission analysis of the Miller cycle with variable cam profile in a pure diesel application

It can be seen from Figure 8 that the application of variable cam profile Miller cycle can significantly reduce NO_x emission with the increase of the Miller degree, and the emission reduction performance is the most obvious under 100% load condition.
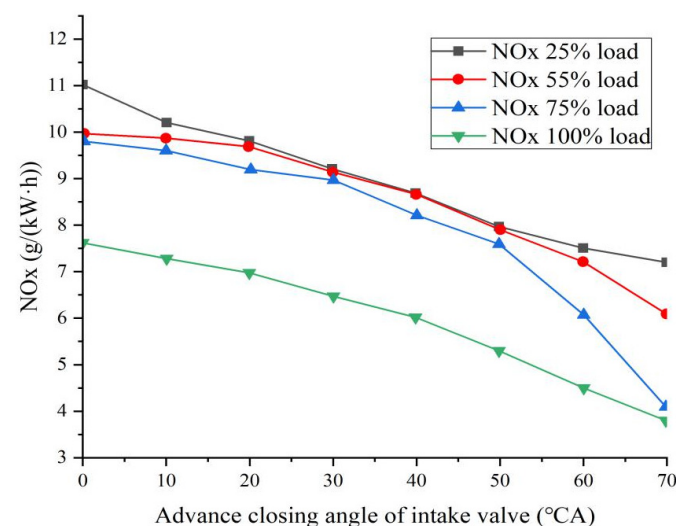
Figure 8. The impacts on NO_x emission when Miller degree > 0.

(2) Emission analysis of the Miller cycle with the overlapping angle of the variable valve in pure diesel

It can be seen from Figure 9 that the effect of variable cam line Miller cycle is similar. The variable valve overlap angle Miller cycle can also significantly reduce NOx emission with the increase of the Miller degree, and its performance is the most obvious under 100% load. This is consistent with the experiment results of Oxenham et al. [56].
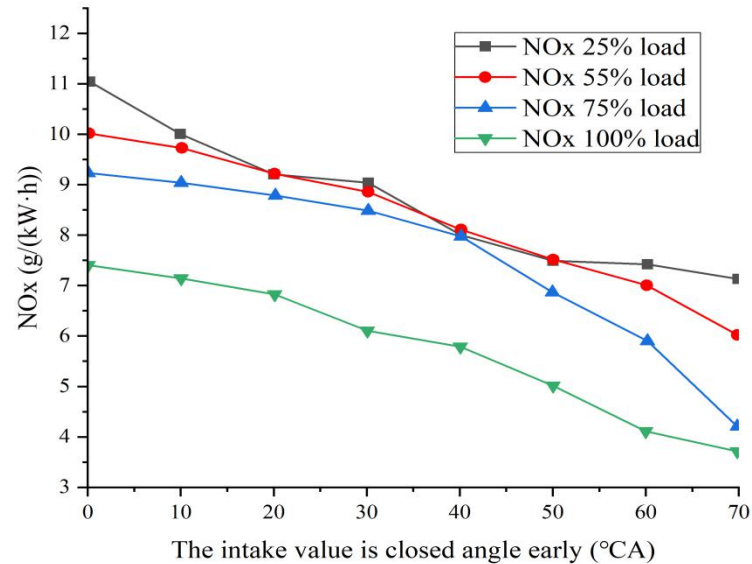
Figure 9. The impact on NO_x emission when Miller degree > 0.

(3) Performance comparison of the two Miller cycle modes in pure diesel

It can be seen from Figure 10 that the effect of variable valve overlap angle Miller cycle is better than that of variable cam line Miller cycle in reducing NO_x emission. With the increase of the Miller degree, the variable overlap angle decreases gradually, which reduces the oxygen content in the cylinder. The variable cam line Miller cycle intake gradually increases, the combustion is sufficient, the temperature increases, and the NO_x emission is large. Therefore, under the same working conditions, the NO_x emission of variable valve overlap angle Miller cycle is lower than that of variable cam line Miller cycle.
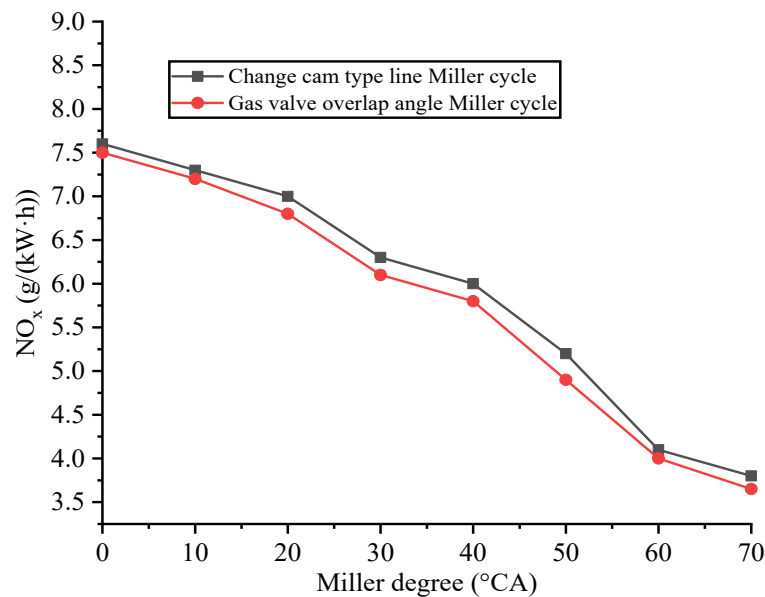
Figure 10. The NO_x emission comparison.

3.5. Performance Comparison of Two Miller Cycle Modes for Biodiesel B10

(1)   Variable valve overlap angle Miller cycle

Figures 11–13 shows the analysis of the effects of variable valve overlap angle Miller cycle on the diesel engine from three aspects of power, fuel consumption, and torque under four different load conditions. Since the NO_x emission performance of pure diesel has been significantly improved after the Miller cycle is applied, NO_x and soot emissions will not be analyzed separately, and the emission results of the two cycles will be compared in the follow-up. There are seven angle changes in the Miller cycle mode in this mode, as shown in Table 8.
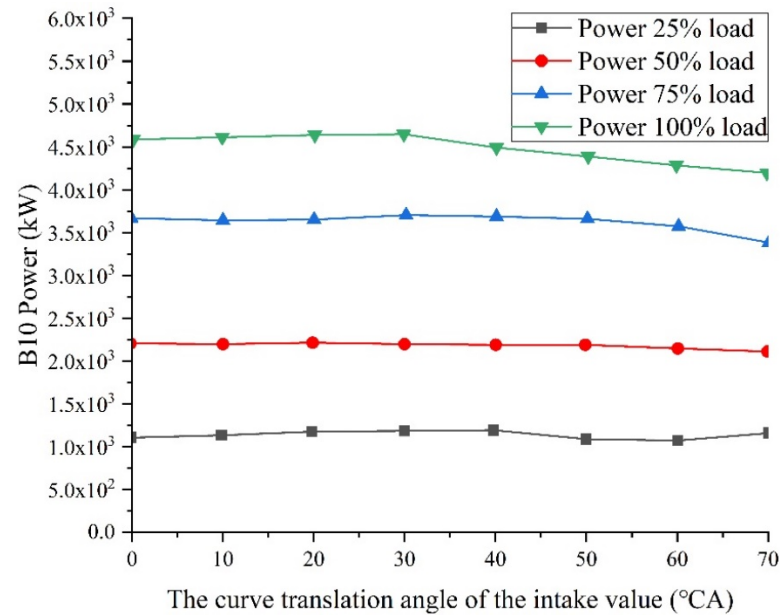

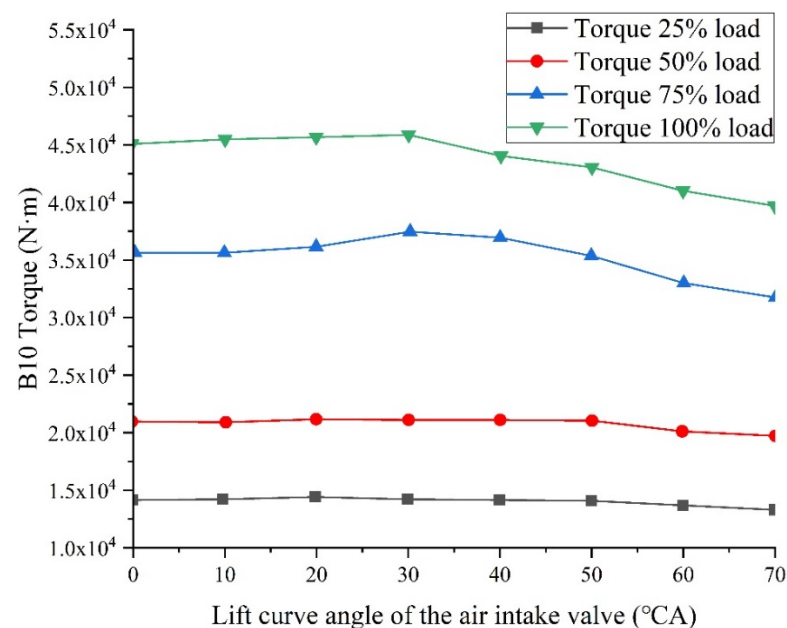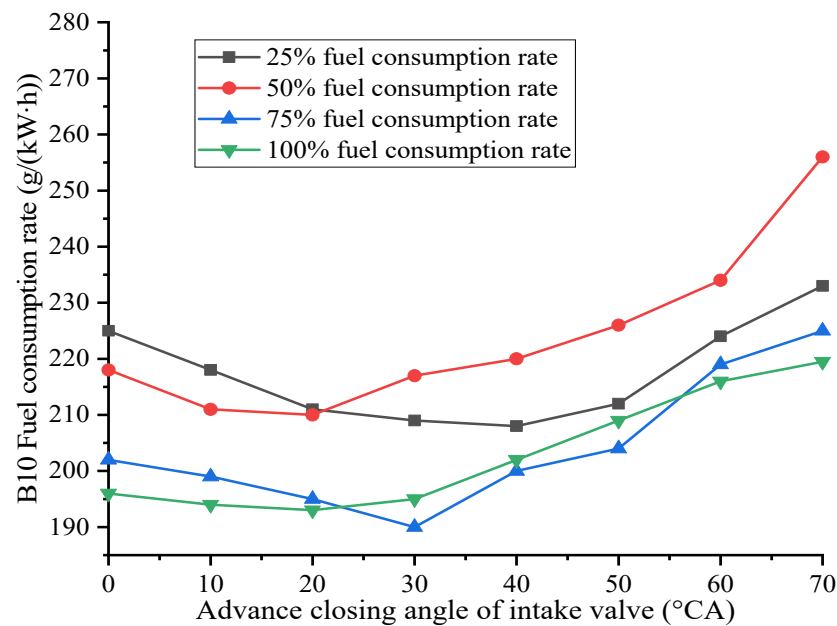**Figure 11.** The power influence when Miller degree > 0.

Figure 12. The torque effect when Miller degree > 0.

Figure 13. The effect of fuel consumption when Miller degree > 0.

The above Figure 11 shows the analysis of the influence of the Miller degree as positive, that is, the advanced closing angle of the inlet valve on the power of this diesel engine. It can be seen from the figure that the power is 100% > 75% > 50% under working conditions. Under four different working conditions of diesel engine, with the gradual increase of intake valve closing angle, the power first increases and then decreases, and there is an inflection point when the Miller degree is 30 °CA. The reason is that when the intake valve closing angle increases in advance, the boost pressure will also increase, and the amount of gas entering the piston-cylinder will increase, its internal combustion is more complete, and then the power increases. However, as the advance angle increases to a certain value, the air volume in the cylinder is excessive, which exceeds the specified amount for the complete combustion of biodiesel, so the power shows a downward trend. This is consistent with the experiment results of Zhang et al. [57].

The above Figure 12 shows that the Miller degree is positive, that is, the inlet valve early closing angle. The torque performance analysis of this diesel engine shows that as the torque change trend is similar to the power trend, it can be obtained from the figure that with the increase of the inlet valve early closing angle, the overall torque first increases slightly and then decreases, and the corner appears when the Miller degree is 30 °CA. The advantages and disadvantages of torque under different working conditions are also similar to power, with the maximum torque under 100% working conditions and the minimum torque under 25% working conditions. The reason is also similar to the power, which will not be repeated here.

The above Figure 13 shows the analysis of the influence of the Miller degree as positive, that is, the advanced closing angle of the inlet valve on the fuel consumption of this diesel engine. It can be seen from the figure that under different working conditions, the fuel consumption of the diesel engine first decreases and then increases with the increase of the advanced closing angle of the intake valve. When the Miller degree is 20 °CA, the fuel consumption performance under the four working conditions can be intuitively identified, which are 100% optimal, 75% secondary, 50% secondary, and 25% worst, respectively. The reason is that the power of the diesel engine is inversely proportional to the fuel consumption curve when the circulating fuel injection quantity is unchanged, that is, the power is large and the fuel consumption is low. When the Miller degree is 20 °CA, the fuel consumption under the four working conditions shows a downward trend. The reasons are as follows: the increase of the Miller degree affects the rise of boost pressure, the air volume in the cylinder increases, the oil–gas mixed combustion is more sufficient and

the combustion is more complete, resulting in the increase of heat released, the increase of external output power of diesel engine and the decrease of fuel consumption. When the Miller degree is greater than 20 °CA, the fuel consumption under various working conditions increases, which is similar to the above power reasons. This is consistent with the experiment results of Guan et al. [58].

(2)   Variable cam profile Miller cycle

In the previous section, the influence of variable valve overlap angle Miller cycle on the performance of B10 Biodiesel Engine in terms of power, fuel consumption, and torque under four conforming working conditions is analyzed. In this section, the performance of the variable cam profile Miller cycle is analyzed based on the conditions in the previous section. In this mode, there are seven angle changes in the Miller cycle mode, as shown in Table 7.

It can be seen from the three figures in Figures 14–16 above that under the four working conditions of 100%, 75%, 50% and 25%, the power, fuel consumption and torque of this diesel engine using the variable cam profile Miller cycle method are the same as those using the variable valve overlap angle Miller cycle. The three key factors are that the effect under 100% load condition is > 75% load condition > 50%, which is consistent with each working condition.
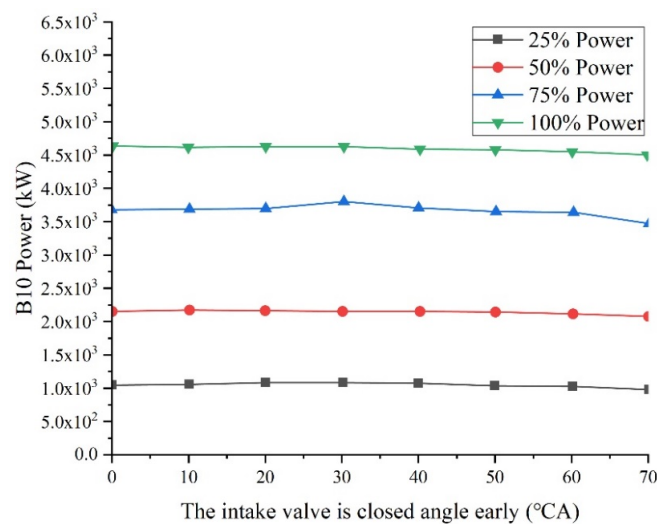

Figure 14. The effect of power influence when Miller degree > 0.
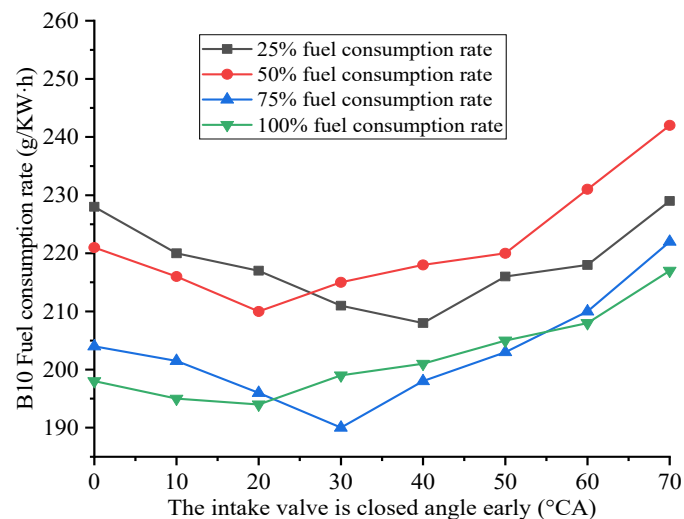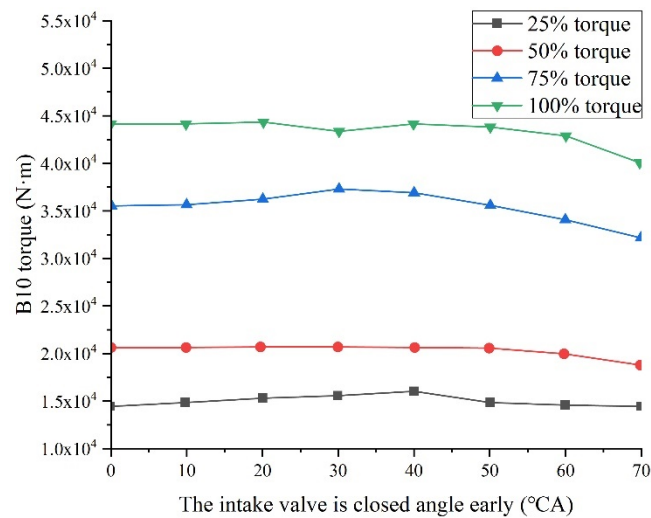

Figure 15. The effect of fuel consumption when Miller degree > 0.

Figure 16. The effect of torque effect when Miller degree > 0.

Based on the analysis of the above two sections, both variable cam profile Miller cycle and variable valve overlap angle Miller cycle can improve its power and reduce fuel consumption, and the Miller degree corner of power and torque appears at 30 °CA. Considering the economy, power, and exhaust emission performance of diesel engines, the optimization effect is the best when the Miller degree is set to 30 °CA under 100% load condition and B10 biodiesel. This is consistent with the experiment results [59].

(3) Comparison of two Miller modes under 100% load condition

Based on the data analysis of various performance indexes of diesel engines by the two Miller methods in the previous two sections, the two Miller methods in this section will compare the five aspects of power, torque, fuel consumption, soot, and NO_x emission under the three conditions of 1000 rpm, B10 concentration biodiesel and 100% load.

It can be seen from Figure 17 that when the Miller degree range is 0–30 °CA, the Miller cycle power of variable cam profile Miller cycle and variable valve overlap angle Miller cycle increase by different degrees. In terms of power value, the Miller cycle of variable valve overlap angle is higher than that of variable cam profile Miller cycle. The reason for the power increase is that when the Miller degree is less than 30 °CA. The intake air of variable cam profile Miller cycle is slightly less than that of variable valve overlap angle Miller cycle because the intake valve lift of the former is shorter and the duration of air entering the cylinder is shorter, while the intake lift of the latter is unchanged, the intake valve overlap angle is smaller, there is less air flowing out of the exhaust passage, the oil–gas mixing of variable valve overlap angle Miller cycle is more sufficient, then the combustion is more complete, and the power is greater. When the Miller degree increases to 40–70 °CA, the power values of both are opposite and tend to decline. The reason for this phenomenon is that the intake volume of the Miller cycle with variable cam profile can increase continuously in the later stage, while the intake volume of the Miller cycle with variable valve overlap angle is insufficient compared with the former in the later stage, resulting in incomplete combustion and black smoke in the diesel engine. The ecological environment is polluted, and the power value also decreases. It is not difficult to see that the overlapping angle Miller cycle power of the variable valve decreases more and more. Therefore, when the Miller degree is 30 °CA, it is the inflection point of power change.
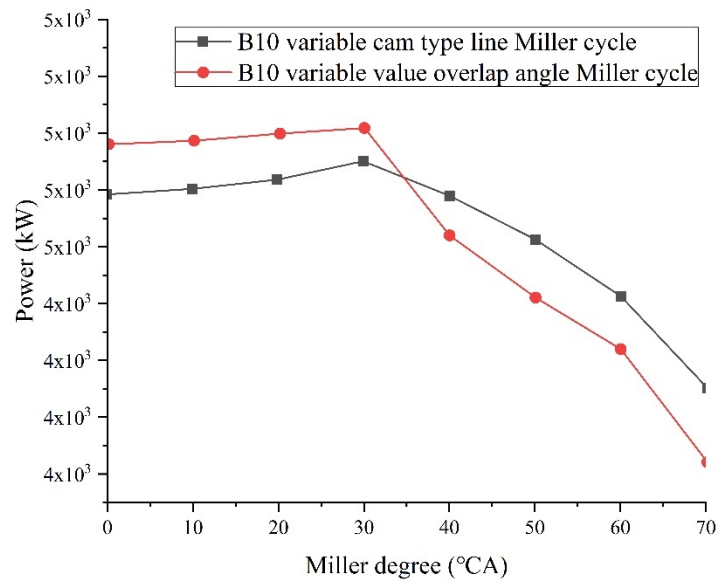
Figure 17. Comparison of two Miller cycles' power.

It can be seen from Figure 18 that when the Miller degree range is 0–30 °CA, the Miller cycle torque value of the overlap angle between the variable cam profile Miller cycle and the variable valve increases by different amplitudes, and the reason for the simultaneous rise is similar to the reason for the rise of the above power value, because there is a certain similar relationship between power and torque The air intake of the Miller cycle with the overlapping angle of variable valve is sufficient during the increase of the Miller degree from 0 to 30 °CA, the oil–gas mixing is more sufficient, the combustion effect is more excellent and the torque value is greater. When the Miller degree increases to 40–70 °CA, the torque values of the two are opposite and tend to decline. The Miller cycle torque value of the variable cam profile is greater than the Miller cycle torque value of the overlap angle of the variable valve. The reduction of the Miller cycle air intake of the overlap angle of the variable valve causes insufficient combustion, and the torque also decreases with the decrease of power, and the reduction range is greater. Therefore, the Miller degree 30 °CA is also the inflection point of torque change of this diesel engine.
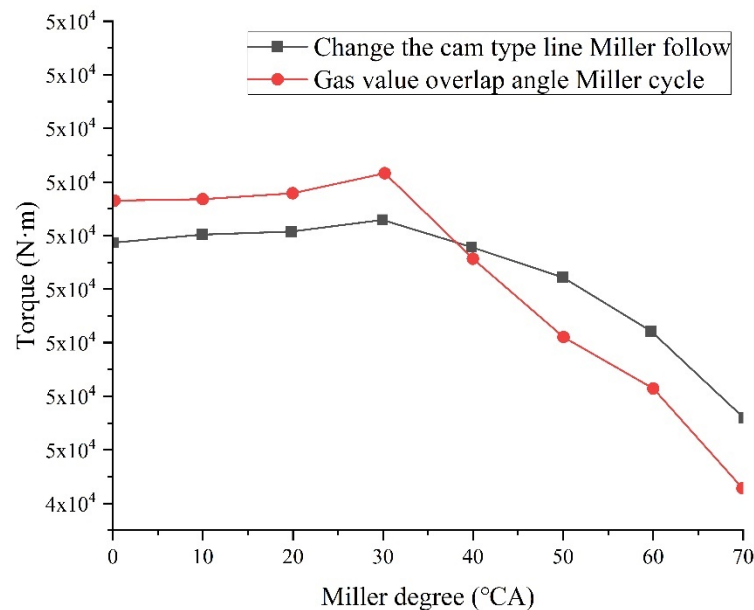

Figure 18. Comparison diagram of two Miller cycle torque.

It can be seen from Figure 19 that when the Miller degree range is 0–20 °CA, the fuel consumption value of Miller cycle with variable cam profile Miller cycle and variable valve overlap angle Miller cycle decreases in different degrees and the fuel consumption performance has been improved in different degrees. The reason is that the air intake of the two Miller cycles increases in different degrees, the oil–gas mixture is sufficient, and the fuel combustion is complete. As the Miller degree increases to 20–70 °CA, the Miller cycle fuel consumption of variable valve overlap angle begins to gradually exceed the Miller cycle fuel consumption of variable cam profile. The main reason for the increase of Miller cycle fuel consumption of variable cam profile is that the cylinder is filled with fresh air with certain heat absorption and cooling effect, resulting in a decrease in temperature, making the increase of fuel consumption small and overlapping with the variable valve. When the Miller degree of valve overlap angle Miller cycle is greater than 30 °CA, the intake air decreases and the oil–gas mixing is insufficient. At this time, to ensure the power performance of diesel engines, vehicle enterprises can only increase the fuel injection during this cycle, which leads to an obvious increase in fuel consumption. Therefore, when the Miller degree is 20 °CA, it is the inflection point of the fuel consumption change of this diesel engine.
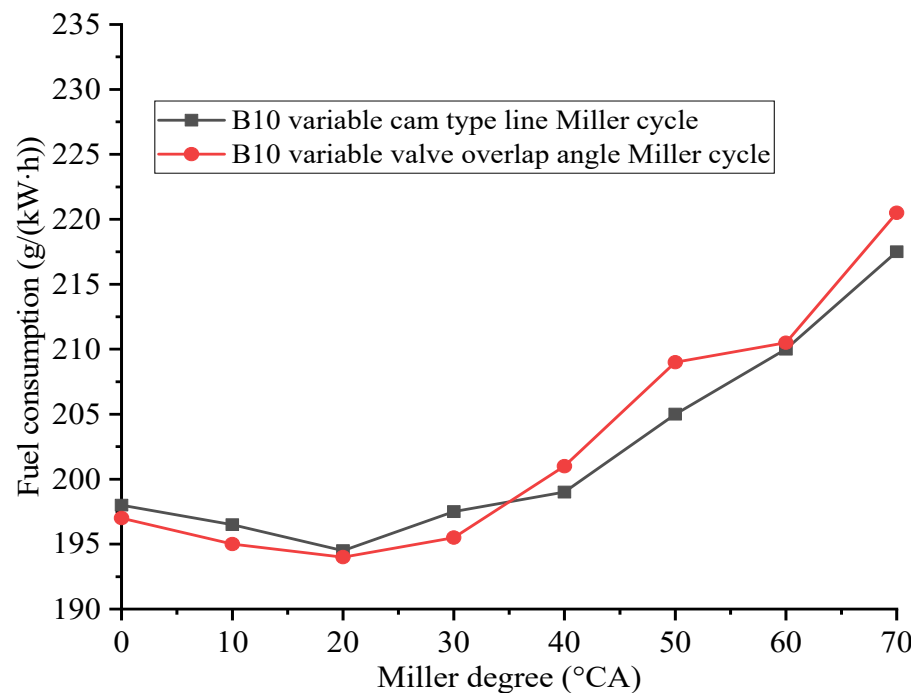

Figure 19. Comparison of fuel consumption of two Miller cycles.

It can be seen from Figure 20 that when the Miller degree range is 0–30 °CA, the soot value of the variable cam line Miller cycle and variable valve overlap angle Miller cycle decreases by different ranges. The soot emission of variable cam profile Miller cycle is slightly higher than that of variable valve overlap angle Miller cycle, which tends to decrease because the fuel combustion is more sufficient and the soot emission decreases. As the Miller degree increases to 30–70 °CA, the soot emission of variable valve overlap angle Miller cycle begins to rise significantly, while the soot emission of variable cam line Miller cycle continues to decline, and the soot emission is far less than that of variable valve overlap angle Miller cycle. The reason for this is that with the increase of the overlap angle of the variable valve, the pressurized incremental air is excluded from the exhaust passage, resulting in the decrease of the intake air volume. On the contrary, the intake of variable cam Miller cycle continues to increase, the combustion of gas and biodiesel in the cylinder is more complete and sufficient, and the soot emission continues to decrease. Therefore,

the Miller degree of 30 °CA is also the turning point of soot emission of the diesel engine after power and torque.
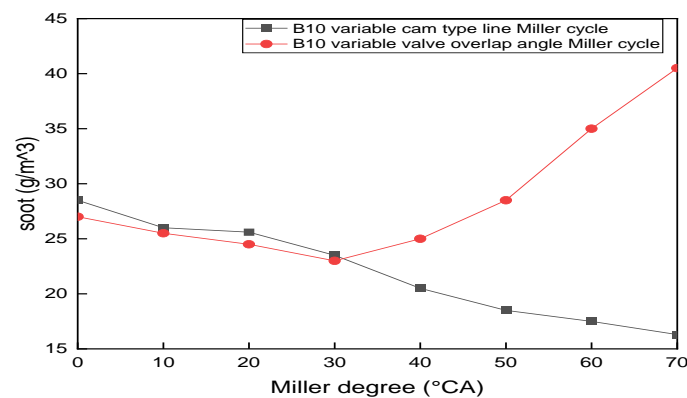

Figure 20. Comparison of soot emission of two Miller cycles.

It can be seen from Figure 21 that under 100% load condition with B10 biodiesel, the NO_x emission of variable valve overlapping angle Miller cycle is lower than that of variable cam profile Miller cycle in the range of the Miller degree 0–70 °CA, which can reflect that the variable valve overlapping angle Miller cycle is significantly better than variable cam profile Miller cycle in reducing NO_x emission performance, and the reasons for reducing NO_x emission are different. With the gradual increase of the Miller degree, the pressure of variable valve overlap angle Miller cycle intake will rise, and the low-pressure gas in the cylinder is difficult to discharge during the exhaust stroke, that is, the high-pressure intake will squeeze the existing waste into the cylinder. With the increase of the Miller degree, the waste content in the cylinder will be greater, and the variable valve overlap Miller cycle intake will gradually decrease, the filling of exhaust gas in the cylinder leads to the reduction of oxygen content, and the final result is the reduction of NO_x emission. With the increase of the Miller degree, there will be an additional expansion period in the intake stroke when the fresh air in the variable cam profile Miller cycle enters the cylinder block and continues until the end of the whole combustion process so that the intake volume of the variable cam profile Miller cycle can continue to increase, the temperature of the fresh gas is low, and it will have a certain cooling effect when entering the cylinder, to reduce NO_x emission. This is similar to the experimental results of Xing et al. [60].
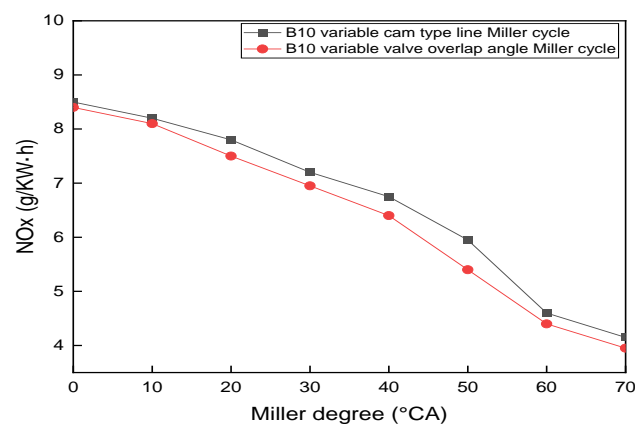

Figure 21. Comparison of NO_x emission of two Miller cycles.

4. Conclusions

With the continuous deterioration of energy crisis [61–65] and environmental problems [66–69], how to effectively reduce engine emissions is the main area of interest for researchers today. Firstly, through the physical and chemical characteristics and tests

of biodiesel, it is concluded that the application of low ratio biodiesel in a diesel engine is the best scheme. Secondly, under different load conditions, the application of the two Miller cycles in a 16V265H diesel engine at 1000 rpm speed is compared, and it is concluded that both can effectively reduce NO_x emission. On this basis, the 16V265H diesel engine at 1000 rpm speed is compared. The main conclusions are as follows:

(1) Through research and analysis, it is found that the change trends of power, fuel consumption and NO_x emission of the 16V265H diesel engine using the two Miller cycles to burn biodiesel under different working conditions are the same, and the smoke emission trend of the Miller cycle with variable valve overlap angle appears an inflection point at 30 °CA under 100% working condition load.

(2) The two Miller cycles can significantly reduce NO_x emission on a 16V265H diesel engine fueled with biodiesel and at 100% load, and the variable valve overlap angle Miller cycle is significantly better than the variable cam profile Miller cycle in reducing NO_x emission.

(3) It can be seen from the above research that under the condition of burning B10 biodiesel and 100% load when the Miller degree increases from 0 °CA to 30 °CA, the variable valve overlap angle Miller cycle is higher in power than the variable cam line Miller cycle, and lower in fuel consumption and soot emission than the variable cam profile Miller cycle.

According to the data analysis, the best scheme is to have the variable valve overlapping angle Miller cycle. When the Miller degree is 30 °CA, the power is the largest and the fuel consumption, soot, and NO_x emissions are the smallest.

Through the above research work, taking the 16V265H diesel engine as an example, the research results of using the Miller cycle technology to burn biodiesel show that for high-power diesel engines (marine, diesel locomotive, heavy truck, etc.), the Miller cycle technology with variable valve overlap angle can effectively improve the comprehensive performance of diesel engines, and it is a cutting-edge technology used to improve its operating performance, which perfectly meets the realization of the vision goal of "carbon neutrality" and has far-reaching significance.

Nomenclature

P	Pressure
T	Temperature
M	Mass
CA	Crankshaft angle
CO	Carbon monoxide
HC	Hydrocarbon
PM	Particulate matter
NO_x	Nitrogen oxides
CO_2	Carbon dioxide
PM	Particulate matter
EGR	Exhaust Gas Re-circulation
IMEP	Indicated mean effective pressure
LIVC	Late intake valve closing
NIE	Net indicated efficiency
EIVC	Early inlet valve closing
RCCI	Reactivity controlled compression ignition
ECU	Electronic control unit
IVO	Intake valve opening
IVC	Intake valve closing
EVO	Exhaust valve opening
B0	100% diesel + 0% biodiesel
B10	90% diesel + 10% biodiesel
B20	80% diesel + 20% biodiesel
B50	50% diesel + 50% biodiesel
B100	0% diesel + 100% biodiesel

References

1. E, J.; Zhang, Z.; Chen, J.; Pham, M.; Zhao, X.; Peng, Q.; Wei, Z.; Yin, Z. Performance and emission evaluation of a marine diesel engine fueled by water biodiesel-diesel emulsion blends with a fuel additive of a cerium oxide nanoparticle. *Energy Convers. Manag.* **2018**, *169*, 194–205. [CrossRef]
2. Cai, T.; Zhao, D.; Wang, B.; Li, J.; Guan, Y. NO emission and thermal performances studies on premixed ammonia-oxygen combustion in a CO2-free micro-planar combustor. *Fuel* **2021**, *280*, 118554. [CrossRef]
3. Peng, Q.; Xie, B.; Yang, W.; Tang, S.; Li, Z.; Zhou, P.; Luo, N. Effects of porosity and multilayers of porous medium on the hydrogen-fueled combustion and micro-thermophotovoltaic. *Renew. Energy* **2021**, *174*, 391–402. [CrossRef]
4. Zhang, Z.; Ye, J.; Lv, J.; Xu, W.; Tan, D.; Jiang, F.; Huang, H. Investigation on the effects of non-uniform porosity catalyst on SCR characteristic based on the field synergy analysis. *J. Environ. Chem. Eng.* **2022**, *10*, 107056. [CrossRef]
5. Cai, T.; Zhao, D. Mitigating NOx emissions from an ammonia-fueled micro-power system with a perforated plate implemented. *J. Hazard. Mater.* **2021**, *401*, 123848. [CrossRef]
6. Canakci, M.; Van, J. Comparison of Engine Performance and Emissions for Petroleum Diesel Fuel, Yellow Grease Biodiesel, and Soybean Oil Biodiesel. *Trans. ASAE* **2003**, *46*, 937–944. [CrossRef]
7. Tan, D.; Chen, Z.; Li, J.; Luo, J.; Yang, D.; Cui, S.; Zhang, Z. Effects of swirl and boiling heat transfer on the performance enhancement and emission reduction for a medium diesel engine fueled with biodiesel. *Processes* **2021**, *9*, 568. [CrossRef]
8. Zhang, Z.; Ye, J.; Tan, D.; Feng, Z.; Luo, J.; Tan, Y.; Huang, Y. The effects of Fe_2O_3 based DOC and SCR catalyst on the combustion and emission characteristics of a diesel engine fueled with biodiesel. *Fuel* **2021**, *290*, 120039. [CrossRef]
9. Li, B.; Li, Y.; Liu, H.; Wang, Z.; Wang, J. Combustion and emission characteristics of diesel engine fueled with biodiesel/PODE blends. *Appl. Energy* **2017**, *206*, 425–431. [CrossRef]
10. Kanaveli, I.; Atzemi, M.; Lois, E. Predicting the viscosity of diesel/biodiesel blends. *Fuel* **2017**, *199*, 248–263. [CrossRef]
11. Zhang, Z.; E, J.; Deng, Y.; Pham, M.; Zuo, W.; Peng, Q.; Yin, Z. Effects of fatty acid methyl esters proportion on combustion and emission characteristics of a biodiesel fueled marine diesel engine. *Energy Convers. Manag.* **2018**, *159*, 244–253. [CrossRef]
12. Zhang, Z.; Tian, J.; Xie, G.; Li, J.; Xu, W.; Jiang, F.; Huang, Y.; Tan, D. Investigation on the combustion and emission characteristics of diesel engine fueled with diesel/methanol/n-butanol blends. *Fuel* **2022**, *314*, 123088. [CrossRef]
13. Georgiou, C.; Azimov, U. Analysis and Multi-Parametric Optimization of the Performance and Exhaust Gas Emissions of a Heavy-Duty Diesel Engine Operating on Miller Cycle. *Energies* **2020**, *13*, 3724. [CrossRef]
14. Cai, T.; Becker, M.; Cao, F.; Wang, B.; Tang, A.; Fu, J.; Han, L.; Sun, Y.; Zhao, D. NOx emission performance assessment on a perforated plate-implemented premixed ammonia-oxygen micro-combustion system. *Chem. Eng.* **2021**, *417*, 128033. [CrossRef]

15. Zhang, Z.; E, J.; Chen, J.; Zhu, H.; Zhao, X.; Han, D.; Zuo, W.; Peng, Q.; Gong, J.; Yin, Z. Effects of low-level water addition on spray, combustion and emission characteristics of a medium speed diesel engine fueled with biodiesel fuel. *Fuel* **2019**, *239*, 245–262. [CrossRef]

16. Poorghasemi, K.; Saray, R.; Ansari, E.; Irdmousa, B.; Shahbakhti, M.; Naber, J. Effect of diesel injection strategies on natural gas/diesel RCCI combustion characteristics in a light duty diesel engine. *Appl. Energy* **2017**, *199*, 430–446. [CrossRef]

17. Lee, C. A Theoretical Study on the Thermodynamic Cycle of Concept Engine with Miller Cycle. *Processes* **2021**, *9*, 1051.

18. Sun, X.; Liang, X.; Zhou, P.; Yu, H.; Cao, X. Computational study of NO x reduction on a marine diesel engine by application of different technologies. *Energy Procedia* **2019**, *158*, 4447–4452. [CrossRef]

19. Xu, Z.; Fu, J.; Liu, J.; Yuan, Z.; Shu, J.; Tan, L. Comparison of in-cylinder combustion and heat-work conversion processes of vehicle engine under transient and steady-state conditions. *Energy Convers. Manag.* **2017**, *132*, 400–409. [CrossRef]

20. Gonca, G.; Sahin, B. Performance analysis of a novel eco-friendly internal combustion engine cycle. *Int. J. Energy Res.* **2019**, *43*, 5897–5911. [CrossRef]

21. Chen, B.; Zhang, L.; Han, J.; Zhang, Q. A combination of electric supercharger and Miller Cycle in a gasoline engine to improve thermal efficiency without performance degradation. *Case Stud. Therm. Eng.* **2019**, *14*, 100429. [CrossRef]

22. Santiago, M.; Antonio, G.; Javier, M.; Daniel, E. Miller cycle for improved efficiency, load range and emissions in a heavy-duty engine running under reactivity-controlled compression ignition combustion. *Appl. Therm. Eng.* **2018**, *136*, 161–168.

23. Wang, P.; Tang, X.; Shi, L.; Ni, X.; Hu, Z.; Deng, K. Experimental investigation of the influences of Miller cycle combined with EGR on performance, energy and exergy characteristics of a four-stroke marine regulated two-stage turbocharged diesel engine. *Fuel* **2021**, *300*, 120940. [CrossRef]

24. Guan, W.; Pedrozo, V.; Wang, X.; Zhao, H.; Ban, Z.; Li, T. Exploring the Potential of Miller Cycle with and without EGR for Maximum Efficiency and Minimum Exhaust Emissions in a Heavy-Duty Diesel Engine. *SAE Int. J. Engines* **2019**, *12*, 579–595. [CrossRef]

25. Wei, S.; Zhao, X.; Liu, X.; Qu, X.; He, C.; Leng, X. Research on effects of early intake valve closure (EIVC) miller cycle on combustion and emissions of marine diesel engines at medium and low loads. *Energy* **2019**, *173*, 48–58. [CrossRef]

26. Li, C.; Wang, Y.; Jia, B.; Roskilly, A. Application of Miller Cycle with turbocharger and ethanol to reduce NOx and particulates emissions from diesel engine—A numerical approach with model validations. *Appl. Therm. Eng.* **2019**, *150*, 904–911. [CrossRef]

27. Demirci, D.; Uyumaz, A.; Sarıdemir, S.; Çınar, C. Performance and Emission Characteristics of a Miller Cycle Engine. *Int. J. Automot. Eng. Technol.* **2018**, *7*, 107–116. [CrossRef]

28. Zhu, S.; Liu, S.; Qu, S.; Deng, K. Thermodynamic and experimental researches on matching strategies of the pre-turbine steam injection and the Miller cycle applied on a turbocharged diesel engine. *Energy* **2017**, *140*, 488–505. [CrossRef]

29. Zhou, S.; Gao, R.; Feng, Y.; Zhu, Y. Evaluation of Miller cycle and fuel injection direction strategies for low NOx emission in marine two-stroke engine. *Int. J. Hydrogen Energy* **2017**, *42*, 20351–20360. [CrossRef]

30. Zhang, Z.; Tian, J.; Li, J.; Ji, H.; Tan, D.; Luo, J.; Jiang, Y.; Yang, D.; Cui, S. Effects of Different Mixture Ratios of Methanol-Diesel on the Performance Enhancement and Emission Reduction for a Diesel Engine. *Processes* **2021**, *9*, 1366. [CrossRef]

31. Yu, X.; She, C.; Farid, G.; Xu, Y. Numerical investigation of a new combined energy cycle based on Miller cycle, Organic Rankine cycle, Stirling engine and alkaline fuel cell. *Energy Rep.* **2021**, *7*, 5406–5419. [CrossRef]

32. Jiang, F.; Cao, W.; Tan, X.; Hu, J.; Zhou, J.; Tan, Z. Optimization Analysis of Locomotive Diesel Engine Intake System Based on Matlab-Simulink and GT-Power. *Processes* **2022**, *10*, 157. [CrossRef]

33. Ma, B.; Yao, A.; Yao, C.; Wu, T.; Wang, B.; Gao, J.; Chao, C. Exergy loss analysis on diesel methanol dual fuel engine under different operating parameters. *Appl. Energy* **2020**, *261*, 114483. [CrossRef]

34. Yadav, J.; Ramesh, A. Injection strategies for reducing smoke and improving the performance of a butanol-diesel common rail dual fuel engine. *Appl. Energy* **2018**, *212*, 1–12. [CrossRef]

35. Cheng, L.; Dimitriou, P.; Weiji, W.; Peng, J.; Aitouche, A. A novel fuzzy logic variable geometry turbocharger and exhaust gas recirculation control scheme for optimizing the performance and emissions of a diesel engine. *Int. J. Engine Res.* **2018**, *21*, 1298–1313. [CrossRef]

36. Wu, B.; Zhao, Q.; Yu, X.; Gu, W.; Zhang, M.; Su, W. Effect of Charge Density on Spray Characteristics, Combustion Process, and Emissions of Heavy-Duty Diesel Engines. *Int. J. Automot. Technol.* **2018**, *19*, 605–614. [CrossRef]

37. Wei, H.; Shao, A.; Hua, J.; Zhou, L.; Feng, D. Effects of applying a Miller cycle with split injection on engine performance and knock resistance in a downsized gasoline engine. *Fuel* **2018**, *214*, 98–107. [CrossRef]

38. He, Y.; Sun, D.; Liu, J.; Zhu, B. Optimization of a turbocharger and supercharger compound boosting system for a Miller cycle engine. *Proc. Inst. Mech. Eng. Part D J. Automob. Eng.* **2018**, *232*, 238–253. [CrossRef]

39. Yan, B.; Wang, H.; Zheng, Z.; Qin, Y.; Yao, M. The effects of LIVC Miller cycle on the combustion characteristics and thermal efficiency in a stoichiometric operation natural gas engine with EGR. *Appl. Therm. Eng.* **2017**, *122*, 439–450. [CrossRef]

40. Wu, B.; Qiang, Z.; Yu, X.; Lv, G.; Nie, X.; Liu, S. Effects of Miller cycle and Variable Geometry Turbocharger on Combustion and Emissions in steady and transient cold process. *Appl. Therm. Eng.* **2017**, *118*, 621–629. [CrossRef]

41. Lin, J.; Xu, Z.; Chang, S.; Yan, H. Finite-time thermodynamic modeling and analysis of an irreversible Miller cycle working on a four-stroke engine. *Int. Commun. Heat Mass Transf.* **2014**, *54*, 54–59. [CrossRef]

42. Afsharizadeh, M.; Mohsennia, M. Novel rare-earth metal oxides-zirconia nanocatalysts for biodiesel production from corn oil and waste cooking oil. *Fuel* **2021**, *304*, 121350. [CrossRef]

43. Sui, M.; Chen, Y.; Li, F.; Wang, H. Study on transition metal ion Fe3+ catalyzed biodiesel oxidation and inhibition mechanism. *Fuel* **2021**, *303*, 121288. [CrossRef]
44. Liu, X.; Xing, S.; Yang, L.; Fu, J.; Lv, P.; Zhang, X.; Li, M.; Wang, Z. Highly active and durable Ca-based solid base catalyst for biodiesel production. *Fuel* **2021**, *302*, 121094. [CrossRef]
45. Corach, J.; Sorichetti, P.; Romano, S. Electrical properties and kinematic viscosity of biodiesel. *Fuel* **2021**, *299*, 120841. [CrossRef]
46. Zhang, Y.; Lou, D.; Hu, Z.; Tan, P. Experimental investigation into the number, micromorphology, functional group composition, and oxidation activity of particles from diesel engine with biodiesel blend. *Fuel* **2021**, *289*, 119902. [CrossRef]
47. Liu, T.; E, J.; Yang, W.; Hui, A.; Cai, H. Development of a skeletal mechanism for biodiesel blend surrogates with varying fatty acid methyl esters proportion. *Appl. Energy* **2016**, *162*, 278–288. [CrossRef]
48. Janakiraman, S.; Lakshmanan, T.; Raghu, P. Experimental investigative analysis of ternary (diesel + biodiesel + bio-ethanol) fuel blended with metal-doped titanium oxide nanoadditives tested on a diesel engine. *Energy* **2021**, *235*, 12148. [CrossRef]
49. Zhou, F.; Wang, J.; Zhou, X.; Qiao, X.; Wen, X. Effect of 2, 5-dimethylfuran concentration on micro-explosive combustion characteristics of biodiesel droplet. *Energy* **2021**, *224*, 120228. [CrossRef]
50. E, J.; Liu, G.; Zhang, Z.; Han, D.; Chen, J.; Wei, K.; Gong, J.; Yin, Z. Effect analysis on cold starting performance enhancement of a diesel engine fueled with biodiesel fuel based on an improved thermodynamic model. *Appl. Energy* **2019**, *243*, 321–335. [CrossRef]
51. Han, D.; E, J.; Deng, Y.; Zhao, X.; Feng, C.; Chen, J.; Leng, E.; Liao, G.; Zhang, F. A review of studies using hydrocarbon reduction measures for reducing hydrocarbon emissions from cold start of gasoline engine. *Renew. Sustain. Energy Rev.* **2021**, *135*, 110079. [CrossRef]
52. Jiang, F.; Li, M.; Wen, J.; Tan, Z.; Zhou, W.; Sivamani, S. Optimization Analysis of Engine Intake System Based on Coupling Matlab-Simulink with GT-Power. *Math. Probl. Eng.* **2021**, *2021*, 1–17. [CrossRef]
53. Huang, Z.; Huang, J.; Luo, J.; Hu, D.; Yin, Z. Performance enhancement and emission reduction of a diesel engine fueled with different biodiesel-diesel blending fuel based on the multi-parameter optimization theory. *Fuel* **2022**, *314*, 122753. [CrossRef]
54. Geng, L.; Bi, L.; Li, Q.; Chen, H.; Xie, Y. Experimental study on spray characteristics, combustion stability, and emission performance of a CRDI diesel engine operated with biodiesel–ethanol blends. *Energy Rep.* **2021**, *7*, 904–915. [CrossRef]
55. Fan, L.; Cheng, F.; Zhang, T.; Liu, G.; Yuan, J.; Mao, P. Visible-light photoredox-promoted desilylative allylation of a-silylamines: An efficient route to synthesis of homoallylic amines. *Tetrahedron Lett.* **2021**, *81*, 153357. [CrossRef]
56. Oxenham, L.; Wang, Y. A Study of the Impact of Methanol, Ethanol and the Miller Cycle on a Gasoline Engine. *Energies* **2021**, *14*, 4847. [CrossRef]
57. Zhang, Z.; E, J.; Chen, J.; Zhao, X.; Zhang, B.; Deng, Y.; Peng, Q.; Yin, Z. Effects of boiling heat transfer on the performance enhancement of a medium speed diesel engine fueled with diesel and rapeseed methyl ester. *Appl. Therm. Eng.* **2020**, *169*, 114984. [CrossRef]
58. Guan, W.; Pedrozo, B.; Zhao, H.; Ban, Z.; Lin, T. Variable valve actuation-based combustion control strategies for efficiency improvement and emissions control in a heavy-duty diesel engine. *Int. J. Engine Res.* **2020**, *21*, 578–591. [CrossRef]
59. Ma, Y.; Liu, C.; E, J.; Mao, X.; Yu, Z. Research on modeling and parameter sensitivity of flow and heat transfer process in typical rectangular microchannels: From a data-driven perspective. *Int. J. Therm. Sci.* **2022**, *172*, 107356. [CrossRef]
60. Xing, K.; Huang, H.; Guo, X.; Wang, Y.; Tu, Z.; Li, J. Thermodynamic analysis of improving fuel consumption of natural gas engine by combining Miller cycle with high geometric compression ratio. *Energy Convers. Manag.* **2022**, *254*, 115219. [CrossRef]
61. Tan, Y.; E, J.; Chen, J.; Liao, G.; Zhang, F.; Li, J. Investigation on combustion characteristics and thermal performance of a three rearward-step structure micro combustor fueled by premixed hydrogen/air. *Renew. Energy* **2022**, *186*, 486–504. [CrossRef]
62. Zuo, H.; Zhang, B.; Huang, Z.; Wei, K.; Tan, J. Effect analysis on SOC values of the power lithium manganate battery during discharging process and its intelligent estimation. *Energy* **2022**, *238*, 121854. [CrossRef]
63. Zuo, H.; Tan, J.; Wei, K.; Huang, Z.; Zhong, D.; Xie, F. Effects of different poses and wind speeds on wind-induced vibration characteristics of a dish solar concentrator system. *Renew. Energy* **2021**, *168*, 1308–1326. [CrossRef]
64. Zuo, H.; Liu, G.; Jiaqiang, E.; Zuo, W.; Wei, K.; Hu, W.; Tan, J.; Zhong, D. Catastrophic analysis on the stability of a large dish solar thermal power generation system with wind-induced vibration. *Sol. Energy* **2019**, *183*, 40–49. [CrossRef]
65. E, J.; Luo, J.; Han, D.; Tan, Y.; Feng, C.; Deng, Y. Effects of different catalysts on light-off temperature of volatile organic components in the rotary diesel particulate filter during the regeneration. *Fuel* **2022**, *310*, 122451.
66. Chen, L.; Deng, Y.; Feng, C.; Han, W.; E, J.; Wang, C.; Han, D.; Zhang, B. Effects of zeolite molecular sieve on the hydrocarbon adsorbent performance of gasoline engine of during cold start. *Fuel* **2022**, *310*, 122427. [CrossRef]
67. Feng, C.; Deng, Y.; Tan, Y.; Han, W.; E, J.; Chen, L.; Han, D. Experimental and simulation study on the effect of ZSM-5 hydrocarbon catcher on the emission of gasoline engine during cold start. *Fuel* **2022**, *313*, 122661. [CrossRef]
68. Li, Y.; Tang, W.; Chen, Y.; Liu, J.; Lee, C.F. Potential of acetone-butanol-ethanol (ABE) as a biofuel. *Fuel* **2019**, *242*, 673–686. [CrossRef]
69. Li, Y.; Meng, L.; Nithyanandan, K.; Lee, T.H.; Lin, Y.; Lee, C.F.; Liao, S. Combustion, performance and emissions characteristics of a spark-ignition engine fueled with isopropanol-n-butanol-ethanol and gasoline blends. *Fuel* **2016**, *184*, 864–872. [CrossRef]